Journal of Alloys and Compounds 507 (2010) 542–546

Contents lists available at ScienceDirect

Journal of Alloys and Compounds

journal homepage: www.elsevier.com/locate/jallcom

Investigation of structural and dielectric behavior of $Eu_2(B'_{0.5}\ B''_{0.5})_2O_7$ (B′ = Ba; B″ = W, Mo) ceramics

N.K. Singh [a], Pritam Kumar [a], O.P. Roy [b], Radheshyam Rai [c,*]

[a] University Department of Physics, V.K.S. University, Ara 802301, Bihar, India
[b] University Department of Physics, B.R.A. Bihar University, Muzaffarpur 842 001, India
[c] Department of Ceramics and Glass Engineering and CICECO, University of Aveiro, 3810-193 Aveiro, Portugal

ARTICLE INFO

Article history:
Received 11 June 2010
Received in revised form 30 July 2010
Accepted 4 August 2010
Available online 12 August 2010

Keywords:
Pyrochlore
X-ray diffraction
Dielectric constant
Cole–Cole plot

ABSTRACT

Defect pyrochlore-type $Eu_2(B'_{0.5}\ B''_{0.5})_2O_7$ (B′ = Ba; B″ = W, Mo) oxides ceramics were prepared by using high-temperature solid-state reaction technique. Preliminary studies of X-ray diffraction (XRD) patterns of the compounds at room temperature suggested that compounds have single phase orthorhombic structures. Studies of dielectric properties (dielectric constant (ε) and tangent loss ($\tan\delta$)) both as a function of frequency (4 kHz to 1 MHz) and temperatures (30–344 °C) does not exhibit dielectric anomaly. The Cole–Cole plot confirms the polydispersive nature of dielectric relaxation of $Eu_2(Ba_{0.5}W_{0.5})_2O_7$ (EBW) and $Eu_2(Ba_{0.5}Mo_{0.5})_2O_7$ (EBM) compounds. Variation of dc resistivity with temperature (94–315 °C) at a constant electric field of 60 V/cm exhibits the semiconductor characteristics of the material.

1. Introduction

Pyrochlore type compounds ($A_2B_2O_7$) have many potential application areas, because of their compositional range, wide variety of interesting electrical, magnetic, optical properties and catalytic behavior [1–5]. Recently some research groups have been recognized as potential candidates for high-temperature, low-loss, high-permittivity dielectric applications [6–9]. These ceramics are suitable for incorporation of aliovalent doping, interstitial oxygen, protons and electronic defects. The crystal structure of most pyrochlore belong to face centred cubic system, with eight molecules per unit cell ($Z = 8$) [10,11]. The A site cations with higher ionic radii has eightfold coordination, with oxygen anions, while the smaller B cation resides in sixfold coordination forming a (BO_6) oxygen octahedron. The ionic radii of A cations range from 0.09 to 0.15 nm and that of B cations ranges from 0.05 to 0.075 nm. For the formation of any pyrochlore compound, there are two criteria: (1) The ratio of the ionic radius of the cation at the A site to that at the B site must be between 1.46 and 1.8 and (2) the chemical valences of various ions must make the compound neutral [12]. The cubic pyrochlore have a general formula $A_2B_2X_6Y$. The B_2X_6 sub-array forms a rigid skeleton of corner-shared octahedra [13–18]. Octahedra are arranged in a tetrahedral array according to a diamond-type net and a system of open channels is observed parallel to the (1 1 0) direction and to that equivalent to cubic symmetry. In a normal pyrochlore, the channel contains an A_2Y' array. The chemical bond between the rigid framework $(BX_3)_n$ and the loose array $(A_2Y')_n$ may be more or less weak. Because of the weak interaction, the A and Y atoms may be partly or completely missing which gives rise to 'defect' pyrochlores [19]. 'Defect' pyrochlores have a B_2X_6 network similar to regular pyrochlore but with vacancies introduced in the A_2Y array. These types of compounds have a tendency of getting contaminated by absorbing moisture from surroundings [13]. The extensive compositional ranges known for pyrochlore compounds reflect the versatility of the A_2O' substructure: "defect" pyrochlores form readily since this network can be partially occupied or even completely absent, as in the pyrochlore-type polymorph of WO_3 (W_2O_6) [20]. Surface energy of bulk materials is negligible as compared with its lattice energy. However, the surface energy contribution becomes more important, or even dominant, as the grain size decreases to very small values, because the ratio of the number of surface atoms to the total number of atoms goes from 10 to 20 or less in bulk materials to values close to unity for small nanoclusters. Particularly for nano-sized materials, grain size is another important factor that affects their structural stability and properties.

Luan et al. [10,11], studied the Bi_2InTaO_7 crystallizes with the pyrochlore-type structure, which acts as a photocatalyst under visible light irradiation and seems to have potential for activity improvement upon modification of its structure. Sellami et al. [21] synthesized the pyrochlore solid solution $Bi_{1.5}Sb_{1.5}Cu_{1-x}Mn_xO_7$ by using ceramic method at 1000 °C. In this paper they reported

* Corresponding author.
E-mail address: radheshyamrai@ua.pt (R. Rai).

0925-8388/$ – see front matter © 2010 Elsevier B.V. All rights reserved.
doi:10.1016/j.jallcom.2010.08.015

that the cell parameter decreases linearly with increasing manganese concentration. Liu et al. prepared $(Gd_{1-x}Yb_x)_2Zr_2O_7$ ceramic powders by using the chemical-coprecipitation and calcinations method. The grain conductivity of this composition gradually increases with increasing temperature from 673 to 1173 K [22].

In view of the importance of the materials and unavailability of the dielectric data, we carried out systematic and extensive studies on structural, dielectric and electrical conducting properties of $Eu_2(Ba_{0.5}W_{0.5})_2O_7$ (EBW) and $Eu_2(Ba_{0.5}Mo_{0.5})_2O_7$ (EBM) ceramics.

2. Experimental procedures

Polycrystalline samples of Europium barium tungstate [Eu2(Ba0.5W0.5)2O7] and Europium barium molybdate [Eu_2(Ba0.5Mo0.5)2O7] oxides were prepared by employing a high-temperature solid-state reaction technique using high purity carbonate and oxides: $BaCO_3$ (99% Burgoyne Buirbridger, India), Eu_2O_3 (99% M/S Indian Rare Earth Ltd.), WO_3 (99% M/S John Baker Inc., USA) and MoO_3, M/S Loba Chemie Pvt. Ltd., India) in required stoichiometry. The mixtures of ingredients of compound EBW and EBM were calcined in alumina crucible at 1100 °C for ~12 h in air atmosphere. The process of grinding and calcination was repeated twice, for the formation of the compounds. The final calcinations were done at 1170 and 1150 °C for tungstate and molybdate compounds, respectively. The homogenous calcined powders of EBW and EBM mixed with binder (polyvinyl alcohol (PVA)) and compacted into cylindrical discs (pellets) of diameter ~10 mm and thickness 1–2 mm at the pressure of 5×10^7 N/m^2 using a hydraulic press. The pellets of EBW and EBM were sintered at 1220 °C for 10 h. The formation and quality of the compounds were checked by X-ray diffraction (XRD) method. The room temperature X-ray diffraction patterns of these compounds were recorded using an X-ray powder diffractometer (Rigaku Miniflex, Japan) using Cu K_α radiation ($\lambda = 0.15418$ nm) in a wide range of Bragg angles 2θ ($20^\circ \leq 2\theta \leq 80^\circ$) with scanning rate 2 °/min. The surface morphology of the gold sputtered samples was recorded with different magnifications at room temperature using a JEOL-JSM-5800 scanning electron microscope (SEM).

The flat polished surfaces of the sintered samples were electroded with air-drying silver paste. Before taking any electrical measurements, the pellets were kept at 150 °C for 2 h. The dielectric constant (ε'), tangent loss ($\tan\delta$) and ac conductivity of the samples were measured as a function of frequency (4 kHz to 100 kHz) at room temperature and temperature (30–344 °C) at two different frequencies (20 and 100 kHz) using a HIOKI 3552 LCR Hi-tester meter (Japan) with a laboratory made three-terminal sample holder. All the measurements were recorded in small temperature intervals (~2 °C) from 30 to 344 °C. The dielectric conductivity/resistivity of compounds were measured as function of temperature (94–315 °C) at constant electric field (60 V/cm) with the help of a KEITHLEY-617 programmable electrometer and laboratory made heating arrangement.

3. Results and discussion

The sharp and single diffraction peaks in room temperature XRD pattern of all the compounds (EBW and EBM) are shown in Fig. 1(a and b). All the peaks were indexed and the cell parameters were determined in different crystal systems using a standard computer program POWDMULT [23]. Finally, a unit cell of orthorhombic crystal system was selected for which $\Sigma\Delta d = (d_{obs} - d_{cal})$ was found to be minimum (standard deviation is 0.0001). A good agreement between the observed and calculated d-values shows the correctness of the selection of crystal system and unit cell parameters. The least-squares refined parameters for EBW and EBM compounds are given in Table 1. The linear particle size (P_{hkl}) of both the samples

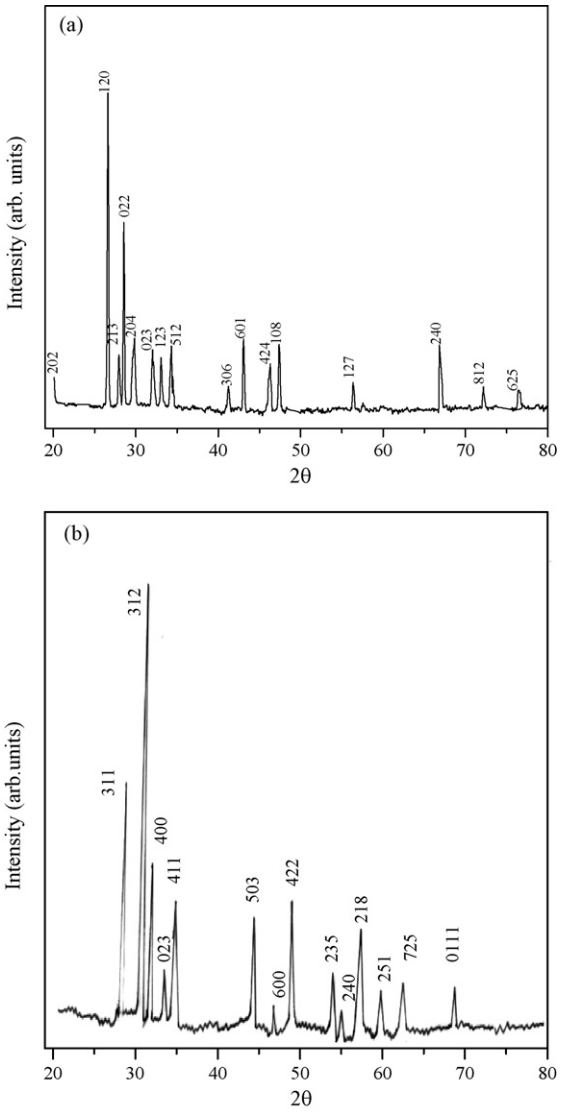

Fig. 1. Room temperature XRD patterns of (a) Eu2(Ba0.5W0.5)2O7 EBW and (b) Eu2(Ba0.5Mo0.5)2O7 EBM samples, respectively.

was calculated from some strong and medium intensity peaks using Scherrer's equation $P_{hkl} = 0.89\lambda/\beta_{1/2}\cos\theta_{hkl}$, where λ is the wavelength of X-ray radiation, $\beta_{1/2}$ the width at half maximum of the diffracted peak and θ_{hkl} the angle of diffraction.

A microstructure study was investigated by scanning electron microscopy. The surface micrographs of the EBW and EBM compounds at same magnification are shown in Fig. 2(a) and (b). The

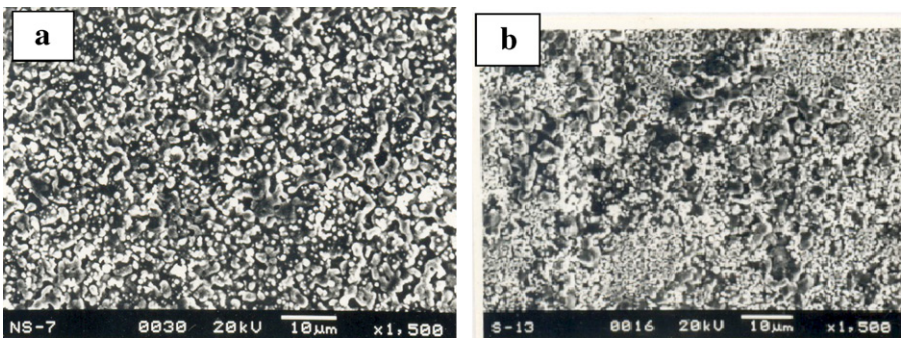

Fig. 2. The SEM micrographs of powder specimens of (a) EBW and (b) EBM compounds.

Table 1
Comparison of observed and calculated *d*-values (in nm) of some reflections of $Eu_2(Ba_{0.5}W_{0.5})_2O_7$ and $Eu_2(Ba_{0.5}Mo_{0.5})_2O_7$ at room temperature.

h	*k*	*l*	d_{obs}	d_{cal}	I/I_0
$Eu_2(Ba_{0.5}W_{0.5})_2O_7$					
3	1	1	3.3387	3.3413	57
3	1	2	3.0841	3.0825	100
4	0	0	2.9609	2.9619	39
0	2	3	2.7968	2.7959	17
4	1	1	2.6788	2.6780	31
5	0	3	2.1034	2.1076	29
6	0	0	1.9746	1.9746	10
4	2	2	1.8953	1.8950	33
2	3	5	1.7127	1.7121	19
2	4	0	1.6837	1.6851	9
2	1	8	1.6156	1.6158	26
2	5	1	1.3619	1.3615	11
7	2	5	1.3357	1.3356	13
0	1	11	1.2384	1.2382	13
$Eu_2(Ba_{0.5}Mo_{0.5})_2O_7$					
2	0	2	4.4285	4.4294	9
1	2	0	3.3510	3.3561	100
2	1	3	3.1922	3.1983	17
0	2	2	3.1264	3.1235	61
2	0	4	2.9641	2.9557	18
4	0	0	2.8847	2.8962	5
4	0	1	2.8356	2.8340	6
0	2	3	2.7799	2.7847	22
1	2	3	2.7103	2.7076	20
5	1	2	2.1011	2.0953	24
3	0	6	1.9689	1.9705	9
6	0	1	1.9122	1.9120	23
4	2	4	1.8751	1.8725	16
1	0	8	1.6995	1.6998	19
1	2	7	1.6952	1.6950	9
2	4	0	1.6780	1.6780	15
8	1	2	1.3885	1.3889	8
6	2	6	1.3602	1.3607	9

SEM micrographs of as-sintered ceramics show a few pores at the grain boundaries. The grain size of EBW and EBM was found to be in the range of 0.1–1.7 and 0.2–2.8 μm, respectively.

The X-ray diffraction data was used to evaluate density (ρ_{XRD}) of the sample using the formula

$$\rho_{XRD} = \frac{\sum A/N}{V} \quad (1)$$

where ρ_{XRD} is the density (gm/cm^2), ΣA is the sum of the atomic weights of all the atoms in the unit cell, N is the Avogadro's number, and V is the volume of the unit cell (cm^3).

The density has been compared with the bulk (measured) density and % of sample porosity using the following relations:

$$\rho_{Bulk} = \frac{\text{mass of the sample pellet}}{\text{volume of the sample pellet}} \quad (2)$$

and

$$\%\,\text{porosity}\,S = \frac{(\text{theoretical density} - \text{measured density}) \times 100}{\text{theoretical density}} \quad (3)$$

The density measurement of EBW and EBM compounds by weight and sample dimension (Eq. (2)) has been compared with theoretical density (XRD density) [24] using the formula of Eq. (3). The results were tabulated in Table 2. The density also reflects the dielectric and loss value of ceramics. Here our dielectric and loss value of ceramics reflect the mixture of 7.4% Air + 92.6% EBW and 8.9% air + 91.1% EBM value.

Fig. 3 shows the frequency (4 kHz to 1 MHz) dependence of relative dielectric constant (ε') and tangent loss ($\tan\delta$) (inset) at room temperature (~30 °C) of EBW and EBM ceramics. It has been observed that the values of the dielectric constant (ε') and tangent loss ($\tan\delta$) of the above compounds decrease with increasing frequency indicating a normal behavior of dielectrics/ferroelectrics. The EBM compound has the highest dielectric constant as compare to EBW compounds. This is due to the presence of all the different types of polarization polarizations (viz. electronic, ionic, interfacial/surface polarization) in the compound at low temperature and frequency [25]. At higher frequency, some of the polarizations were getting ineffective and hence, at higher frequency we have lower value of ε'. In the case of $\tan\delta$, it is very similar nature like that of dielectric constant. Tangent loss ($\tan\delta$) decreases rapidly up to 20 kHz and becomes almost constant afterwards. This behavior is also found in other compounds of the family studied by us in their ceramic form [26,27,16].

Table 2
Comparison of structural parameters and dielectric properties of compounds $Eu_2(Ba_{0.5}W_{0.5})_2O_7$ and $Eu_2(Ba_{0.5}Mo_{0.5})_2O_7$.

Parameters	$Eu_2(Ba_{0.5}W_{0.5})_2O_7$	$Eu_2(Ba_{0.5}Mo_{0.5})_2O_7$
a (nm)	1.1847(6)	1.1584(9)
b (nm)	0.7030(8)	0.7012(8)
c (nm)	1.3836(5)	1.3747(2)
ε'_{RT} at 20 kHz	41	96
ε'_{RT} at 100 kHz	37	84
$\tan\delta_{RT}$ at 20 kHz	0.14	0.67
$\tan\delta_{RT}$ at 100 kHz	0.07	0.33
ε'_{max} at 20 kHz	45	167
ε'_{max} at 100 kHz	41	132
$\tan\delta_{max}$ at 20 kHz	2.22	4
$\tan\delta_{max}$ at 100 kHz	1.37	2
α_ε (ppm/°C) at 20 kHz	29	93
α_ε (ppm/°C) at 100 kHz	62	45
ρ_{XRD} (gm/cc)	7.24	6.16
ρ_{bulk} (gm/cc)	6.70	5.61
S (%)	7.4	8.92

Fig. 4 shows the variation of ε' for EBW and EBM compounds with temperature (30–320 °C) at frequencies 20 and 100 kHz. In case of EBM compound the value of ε' increasing with temperature and rate of increase is much faster at 20 kHz than that of 100 kHz. Similar increasing trend at higher temperature (>270 °C) is observed in EBM compound. Dielectric constant (ε') (in both EBW and EBM) increases slowly up to temperature 280 °C at 20 and 100 kHz then after increases rapidly in EBW compound. In inset of Fig. 4 shows the variation of tangent loss ($\tan\delta$) for EBW and EBM compounds with temperature (30–320 °C) at frequencies 20 and

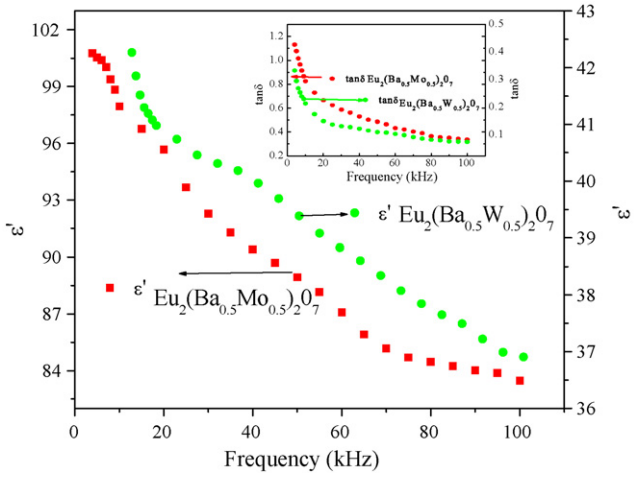

Fig. 3. Variation of relative dielectric constant (ε') of Eu2(Ba0.5W0.5)2O7 and Eu2(Ba0.5Mo0.5)2O7 with frequency at room temperature and variation of tangent loss ($\tan\delta$) of Eu2(Ba0.5W0.5)2O7 and Eu2(Ba0.5Mo0.5)2O7 with frequency at room temperature (in inset).

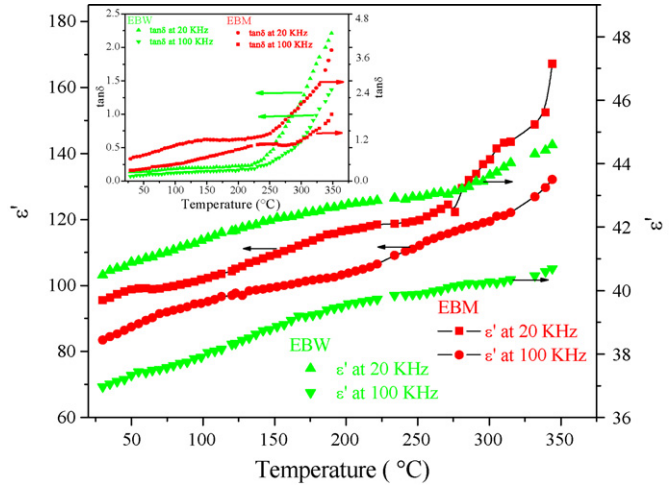

Fig. 4. Variation of dielectric constant (ε') of Eu2(Ba0.5W0.5)2O7 and Eu2(Ba0.5Mo0.5)2O7 with temperature at frequencies 20 and 100 kHz and variation of tangent loss ($\tan\delta$) with temperature at frequencies 20 and 100 kHz (in inset).

100 kHz. In case of EBM compound the value of loss tangent ($\tan\delta$) increasing with temperature. The rate of increase is much faster at 20 kHz than that of 100 kHz at higher temperature (>270 °C) in EBM compound. In the case of in EBW compound, $\tan\delta$ remains almost constant up to 215 °C, afterwards, it increases much faster at 20 kHz than that of 100 kHz [28]. We compare the dielectric data of the compounds at different frequencies and temperatures in Table 2.

One of the most convenient ways to check the polydispersive relaxation in EBW and EBM compounds is complex Argand plane plots of ε'' against ε', usually called Cole–Cole plots [29]. For a pure monodispersive Debye process, one expects semicircular plots with the centre located on the ε'-axis, whereas, for polydispersive relaxation these Argand plane plots are close to circular arc with end points on the axis of reals and the centre below this axis. The complex dielectric constant in such situations is known to be described by the empirical relation [29] given as

$$\varepsilon* = \varepsilon' - j\varepsilon'' = \varepsilon_\infty + \frac{(\varepsilon_s - \varepsilon_\infty)}{1 + (j\omega\tau)^{1-\alpha}}$$

where ε_s and ε_∞ are the low and high frequency values of ε' and α is a measure of the distribution of relaxation times, which can be determined from the location of the centre of Cole–Cole circle of which only an arc lies above the ε'-axis. We have plotted ε'' against ε' in the Fig. 5(a) and (b) at 30 °C. It is evident from this plot that the relaxation process differs from the monodispersive Debye process (for which $\alpha = 0$) and found to be 0.32 for EBW and 0.41 for EBM compounds. This value of α from Cole–Cole plot confirms the polydispersive nature of dielectric relaxation of EBW and EBM compounds.

The variation of measured ac conductivity ($\ln\sigma_{ac}$) of the EBW and EBM compounds at 20 and 100 kHz with inverse of absolute temperature ($1/T$) is shown in Fig. 6. The temperature dependence of ac electrical conductivity σ_{ac} and activation energy (E_a) of the EBW and EBM compounds were calculated from the impedance data collected with an LCR meter and using the formula [30,31]

$$\sigma = \omega\varepsilon_0\varepsilon' \tan\delta \quad \text{and Arrhenius law : } \sigma_{ac} = \sigma_0 \exp(-E_a/k_B T)$$

where ω is the angular frequency, ε_o is the vacuum permittivity and k_B is the Boltzmann constant. In both the compounds conductivity of the compound at higher temperature is higher, which is common behavior of most of the dielectric ceramics. The value of the activation energy E_a has been calculated from the slope of the graph

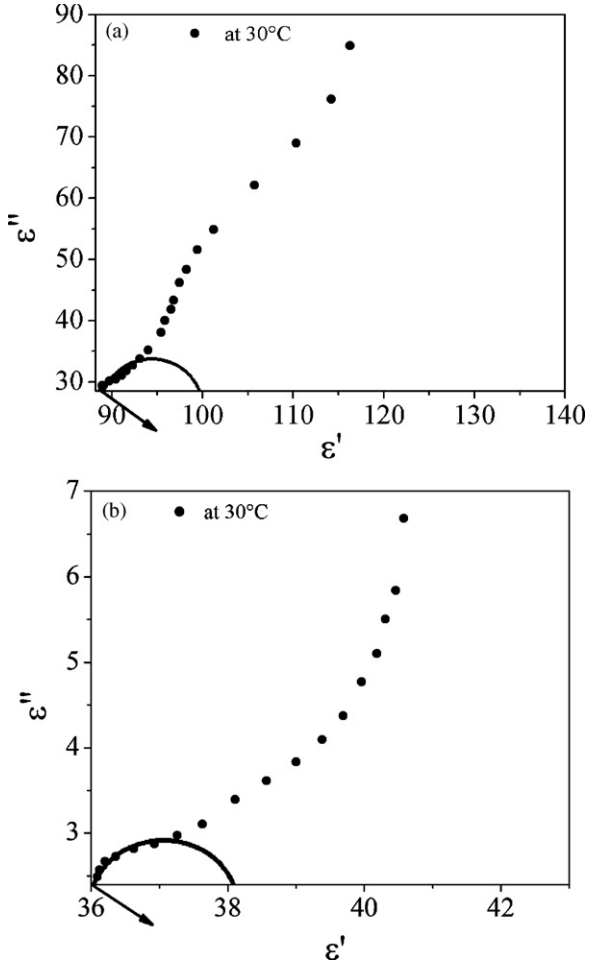

Fig. 5. Complex Argand plane plots of ε'' against ε' of (a) Eu2(Ba0.5W0.5)2O7 and (b) Eu2(Ba0.5Mo0.5)2O7 at 30 °C.

in high-temperature region (>327 °C) and was found to be 0.11 eV for EBW compound and 0.09 eV for EBM compound at 100 kHz. The low values of activation energy support the superionic nature of the compounds in the high-temperature region. The variation of dc

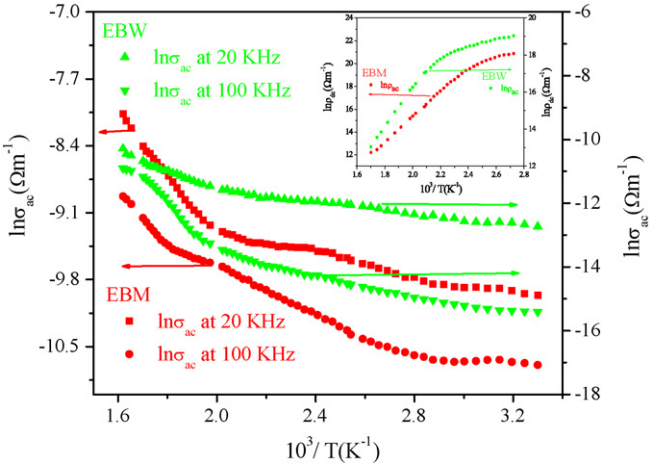

Fig. 6. Variation of ac conductivity ($\ln\sigma_{ac}$) of Eu2(Ba0.5W0.5)2O7 and Eu2(Ba0.5Mo0.5)2O7 with inverse of absolute temperature ($1/T$) at frequencies 20 and 100 kHz and variation of dc resistivity with inverse of absolute temperature ($1/T$) of Eu2(Ba0.5W0.5)2O7 and Eu2(Ba0.5Mo0.5)2O7 compounds (in inset).

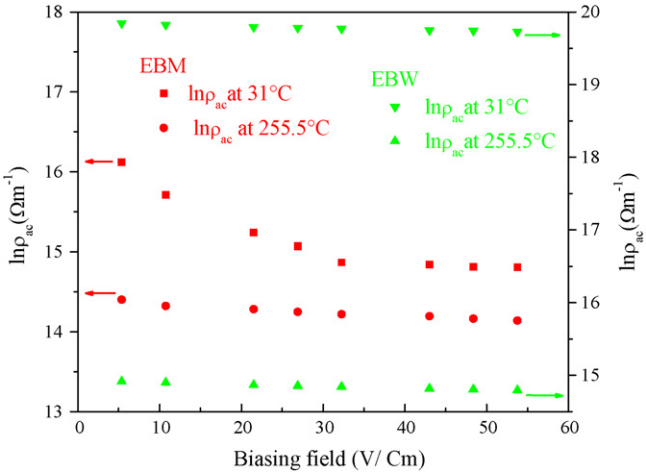

Fig. 7. Variation of dc resistivity of Eu2(Ba0.5W0.5)2O7 and Eu2(Ba0.5Mo0.5)2O7 as a function of biasing field at temperatures 31 and 255.5 °C.

resistivity of the EBW and EBM compounds with inverse of absolute temperature ($1/T$) at constant electric field (60 V/cm) is shown in inset of Fig. 6. The resistivity decreases with increasing temperature which can be due to creation of free electrons due to thermal energy [32,33].

Fig. 7 shows the variation of dc resistivity ($\ln \rho$) with applied field (1–80 V/cm) of both the tungstate and molybdate compounds at 31 °C and 255.5 °C. It shows that the dc resistivity of EBW and EBM compounds decreases with increasing biasing field due to the following. (a) Ionization occurs in inhomogeneous dielectric solids mainly through the mechanism of partial discharge of gases or moisture from pores or cracks present in the ceramic. The electric field results in the generation of local heat causing the generation of thermal stresses and increased conduction locally. The stresses can generate cracks, leading to further ionization up to a certain field. (b) Electrons may be ejected from the electrode materials. These electrons are then accelerated through the sample and collide with ions or atoms in the solid knocking out other electrons and ionization takes place. Therefore, resistivity decreases and conductivity increases as the biasing field increases [34].

4. Conclusions

Finally, it can be concluded that above-mentioned pyrochlore-type compounds have an orthorhombic crystal structure at room temperature (~30 °C). Scanning electron microscopy (SEM) was used to analyze the surface morphology of the samples. Studies of the dielectric constant and dielectric loss of compound as a function of frequency (4 kHz to 1 MHz) at room temperature and temperature (30–344 °C) at 20 and100 kHz suggest that the compound do not have dielectric anomaly in the studied frequency and temperature ranges. EBW compound has the highest dielectric constant as compare to EWM compound. The complex Argand plane plot of ε'' against ε', usually called Cole–Cole plots is used to check the polydispersive nature of relaxation phenomena in above-mentioned compounds. A relaxation phenomenon of non-Debye type has been observed in the EBW and EBM compounds. The value of the activation energy E_a was found to be 0.11 eV for EBW compound and 0.09 eV for EBM compound. The low values of activation energy support the superionic nature of the compounds in the high-temperature region.

Acknowledgements

Authors are thankful to Prof. R.N.P. Choudhary, IIT Kharagpur for his technical support, discussions and valuable suggestions extended during this work.

References

[1] M.A. Subramanian, A.W. Sleight, in: K.A. Gschneider, I. Erying (Eds.), Handbook on the Physics and Chemistry of Rare Earths, vol. 8, Elsevier Science Publishers, Oxford, UK, 1993, p. 642.
[2] C. Bansal, H. Kawaanaka, H. Bando, Y. Nishihara, Physica B 329 (2003) 1034.
[3] D.P. Cann, C.A. Randall, C.A. Shrout, Solid State Commun. 100 (1996) 529.
[4] F.W. Poulsen, M. Glerup, P. Holappels, Solid State Ionics 135 (2000) 595.
[5] J.B. Goodenough, R.N. Castellano, J. Solid State Chem. 44 (1982) 108.
[6] A.V. Chadwick, Nature (London) 408 (2000) 925.
[7] J.B. Goodenough, Nature (London) 404 (2000) 821.
[8] P. Lacorre, F. Goutenoire, O. Bohnke, R. Petoux, Y. Laligant, Nature (London) 404 (2000) 856.
[9] D.P. Cann, C.A. Randall, T.R. Shrout, Solid State Commun. 7 (1996) 529.
[10] J. Luan, W. Zhoo, J. Feng, H. Cai, Z. Zheng, B. Pan, X. Wu, Z. Zou, Y. Li, J. Hazard. Mater. 164 (2009) 781.
[11] J. Luan, K. Ma, B. Pan, Y. Li, X. Wu, Z. Zou, J. Mol. Catal. A: Chem. 321 (2010) 1.
[12] P.P. Rao, K.R. Nair, P. Koshy, V.K. Vaidyan, J. Mater. Sci. Mater. Electron. 17 (2006) 497.
[13] J.B. Goodenough, H.Y.-P. Hong, J.A. Kafalas, Mater. Res. Bull. 11 (1986) 203.
[14] C.M. Mari, F. Bonino, M. Catti, R. Pasinetti, S. Pizzini, Solid State Ionics – Diffus. React. 18/19 (1986) 1013.
[15] A. Tiwari, M. Prabaharan, R.R. Pandey, S. Li, J. Inorg. Organomet. Polym. 20 (2010) 380–386.
[16] N.K. Singh, P. Kumar, H. Kumar, R. Rai, Adv. Mater. Lett. 1 (2010) 79–82.
[17] A. Tiwari, S. Li, Polym. J. 41 (2009) 726–732.
[18] R. Rai, Adv. Mater. Lett. 1 (2010) 55–58.
[19] D. Babel, G. Pausewang, W. Viebahn, Z. Naturforsch. 22b (1967) 1219.
[20] A.R. Heredia, M.Q. García, J.L.P. Mazariego, R. Escamilla, doi:10.1016/j.jallcom.2010.05.143.
[21] M. Sellami, V. Caignaert, M. Hamdad, A. Bekka, N. Bettahar, J. Alloys Compd. 482 (2009) 13.
[22] Z.G. Liu, J.H. Ouyang, Y. Zhou, X.L. Xia, J. Alloys Compd. 490 (2010) 277.
[23] E. Wu, "POWD", An Interactive Powder Diffraction Data Interpretation and Indexing Program, Version 2.1, School of Physical Science, Flinders University of South Australia Bedford Park, SA 5042, Australia.
[24] B.D. Cullity, Elements of X-ray Diffraction, Addison-Wesley Publishing Company, Philippines, 1978.
[25] J.C. Anderson, Dielectrics, Chapman & Hall, London, 1964.
[26] Z.X. Cheng, X.L. Wang, G. Alvarez, S.X. Dou, S.J. Zhang, T.R. Shrout, J. Appl. Phys. 105 (2009) 07D902.
[27] N.K. Singh, R.N.P. Choudhary, B. Behera, Physica B 403 (2008) 1673.
[28] T. Kar, R.N.P. Choudhary, Mater. Sci. Eng. B 90 (2002) 224.
[29] K.S. Cole, R.H. Cole, J. Chem. Phys. 9 (1941) 341.
[30] N.K. Singh, S. Sharma, R.N.P. Choudhary, Indian J. Phys. 74B1 (2000) 63.
[31] V.M. Qurevich, Electric Conductivity of Ferroelectrics, Moskva, 1969.
[32] R.C. Buchann, Ceramic Materials for Electronics, Marcel Dekker Inc., New York, 1986, p. 77.
[33] R.A. Weeks, E. Sonder, J. Am. Ceram. Soc. 63 (1980) 92.
[34] B. Tareev, Physics of Dielectric Materials, Mir Publishers, Moscow, 1979, p. 60.